Supporting Information

Few-Layer ZnO Nanosheets: Preparation, Properties, and Films with Exposed {001} Facets

Jan Demel,[a] Josef Pleštil,[b] Petr Bezdička,[a] Pavel Janda,[c] Mariana Klementová,[a] and Kamil Lang[a,*]

[a] *Institute of Inorganic Chemistry, v.v.i., Academy of Sciences of the Czech Republic, 250 68 Řež (Czech Republic)*

[b] *Institute of Macromolecular Chemistry, v.v.i. Academy of Sciences of the Czech Republic, Heyrovského nám. 2, 162 06 Praha (Czech Republic)*

[c] *J. Heyrovský Institute of Physical Chemistry, v.v.i., Academy of Sciences of the Czech Republic, Dolejškova 3, 182 23 Praha (Czech Republic)*

* Corresponding author, lang@iic.cas.cz

Table of Contents

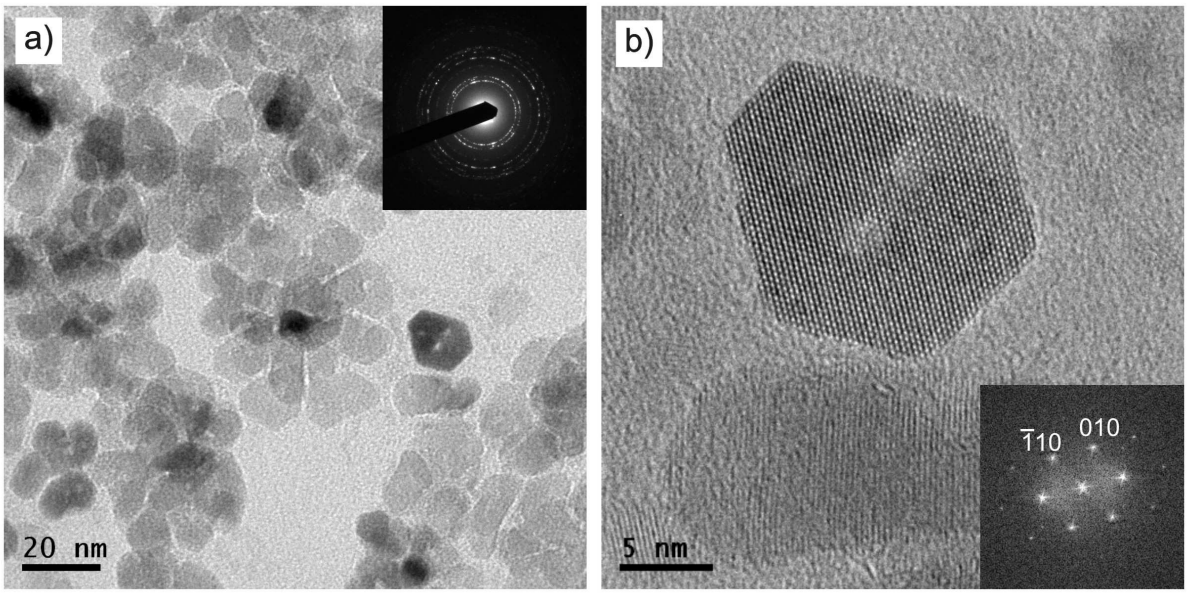

Figure S1. HRTEM observations of the ZnO nanosheets prepared at 80°C: (a) Bright-field image with the electron diffraction pattern in the inset; (b) High-resolution image of a single crystal viewed along the [001] direction with FFT in the inset.

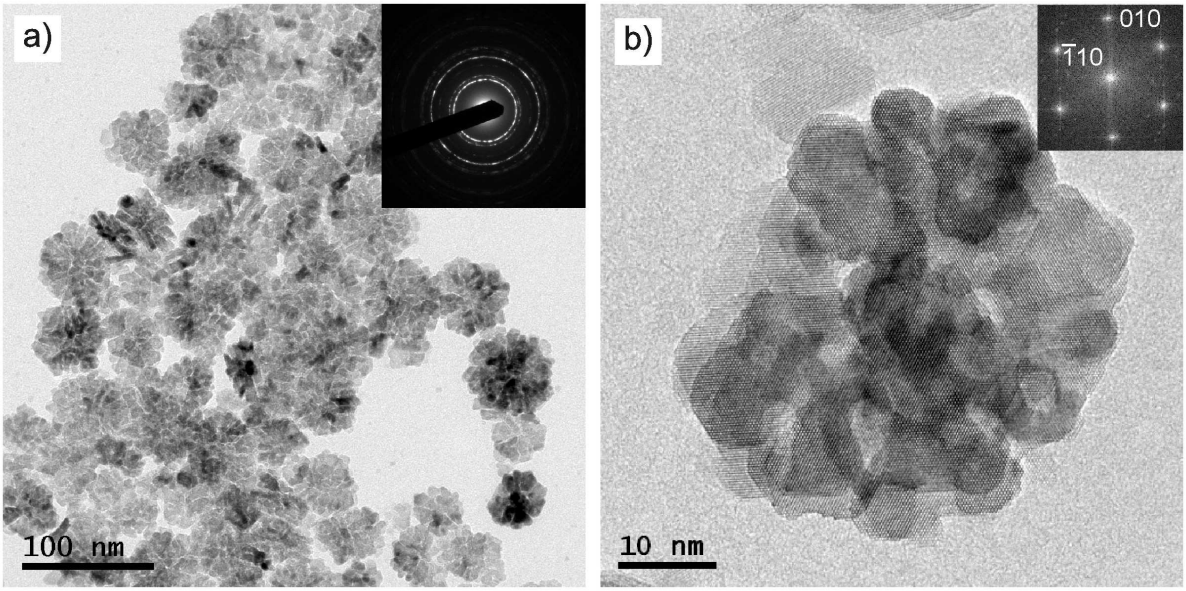

Figure S2. HRTEM observations of the ZnO nanosheets prepared by shaking in *n*BuOH at 60°C: (a) Bright-field image with the electron diffraction pattern in the inset; (b) High-resolution image of a single crystal viewed along the [001] direction with FFT in the inset.

Detailed discussion of AFM results

The axial height of the single sheets is ~0.6–0.7 nm. To understand the axial measure, it should be noted that while the axial coordinate is unaffected by AFM tip-shape convolution, it can be deformed by the force exerted by an AFM tip upon axial loading on an AFM cantilever. Depending on compressibility of the nanoparticle, the displayed axial measure may vary to some extent, which can be a source of variation in the axial dimensions found for different nanoparticle units. It is noteworthy that no differences of statistical importance were found in the surface nanoparticle distribution density of the AFM images acquired in the tapping and contact modes. This result implies good nanoparticle adhesion to the mica surface, which allows for the performance of high-resolution contact AFM imaging.

The studied ZnO nanoparticles (colloids prepared at 60 and 100 °C) are mostly aggregates. Approximately 10 % of the total amount of nanoparticles (as determined by investigation of representative surface locations) represent single non-aggregated units, while the rest of the particles are particles grown in both lateral and axial directions, i.e., combined 2D–3D aggregates. The composition of the basic units is clearly resolved on quasi-2D aggregates (Figure S3, Figure S4). The axial measure (height) of these aggregates corresponds to two or three nanoparticle units as indicated by the profile analysis of the AFM topography (Figure S5). The height of the 3D aggregates exceeds 2 nm, approaching 3 nm, which corresponds to a higher degree of axial stacking (up to 3–4 units). A lateral measure of ~60 nm (convoluted) leads to the assumption of planar close-packed aggregates of ~3 units. Other illustrations of the nanoparticle morphology are given in Figures S6, S7, and S8.

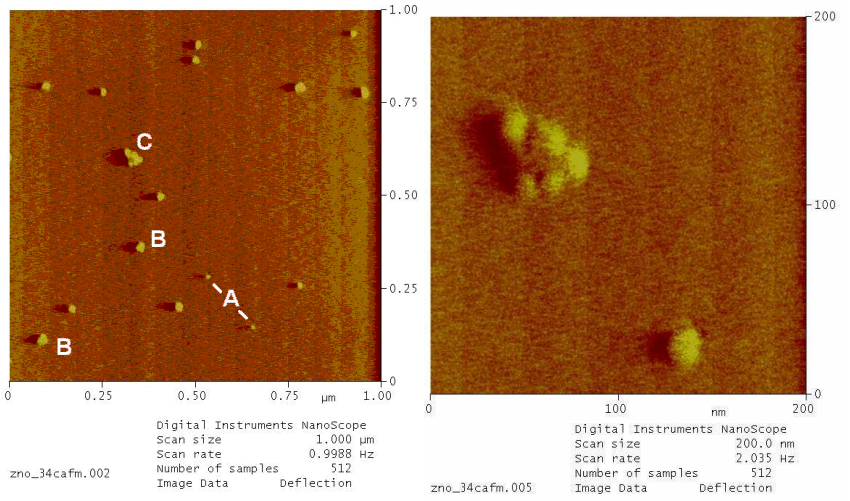

Figure S3: Contact AFM image of the ZnO nanoparticles prepared at 60 °C in *n*BuOH. The left image shows single units (A), 3D aggregates with preferable axial stacking and minor lateral aggregation (B), and quasi-2D aggregate with preferable lateral aggregation of the nanoparticle units (C). The quasi-2D aggregate (C) is resolved in the zoomed image (right).

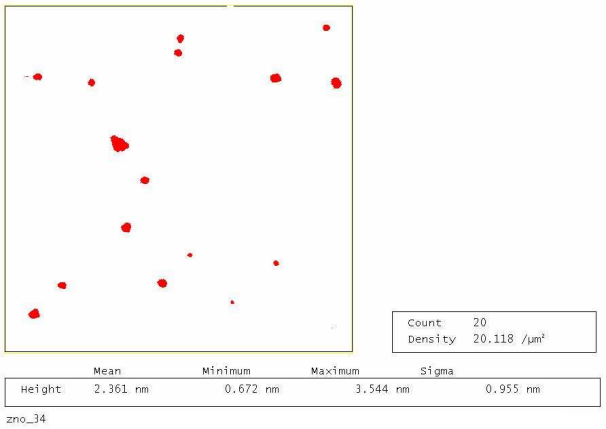

Figure S4: Overview of the ZnO nanoparticles prepared at 60 °C in *n*BuOH (AFM contact, particle analysis) showing the range of heights. It indicates one- to five-sheet stacked aggregates.

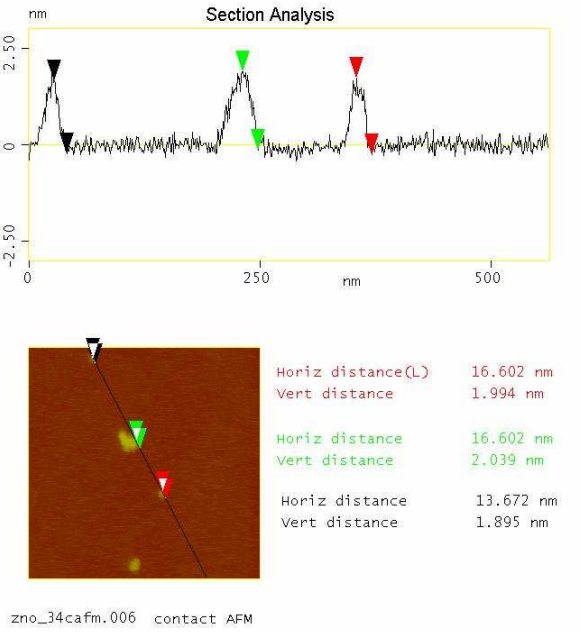

Figure S5: Profile analysis of the large quasi-2D aggregate (green markers) shown in Figures S3 and S4. Another two aggregates (red and black markers), both with an axial measure ~2 nm, indicate two- or three sheet vertical stacking. Their lateral size < 20 nm (convoluted with an AFM tip) represents the lowest lateral measure found for single nanoparticles.

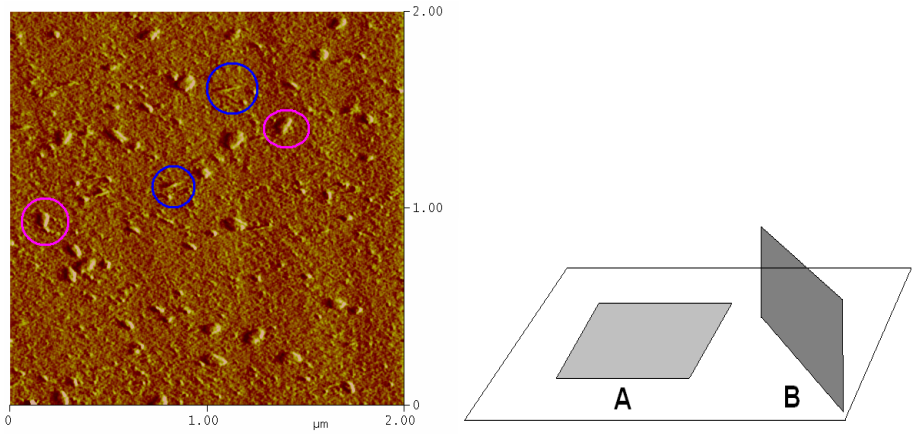

Figure S6. AFM image (contact mode, deflection) of the ZnO nanoparticles prepared at 100°C in *n*BuOH and deposited on a mica surface. The side (blue circles, *B* in the scheme) and planar orientations (magenta circles, A in the scheme) of the sheets are clearly resolved.

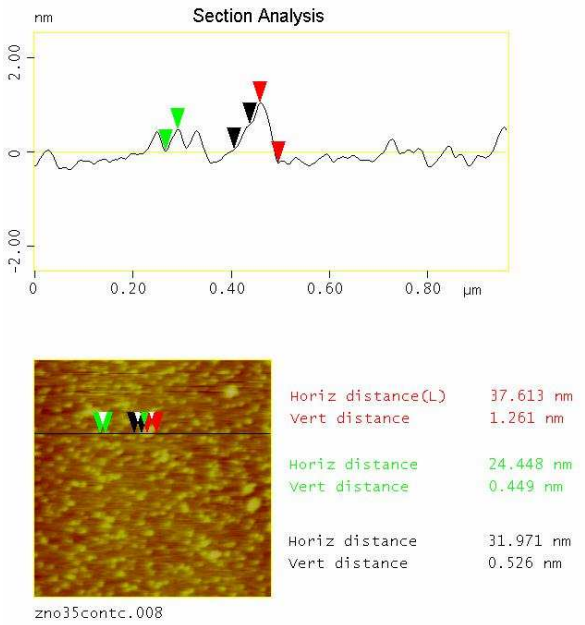

Figure S7. AFM topographic profile analysis of the ZnO nanoparticles prepared at 100°C in *n*BuOH. The ZnO sheets of the unit thickness (~0.6 nm) form axial aggregates with a multiple height.

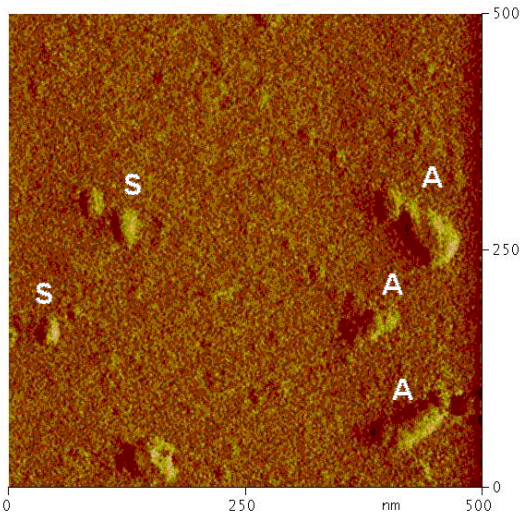

Figure S8: AFM image (contact, deflection) of the ZnO nanoparticles prepared at 100°C in *n*BuOH. The single units (S) and their planar side-by-side aggregates (A) are well resolved.

Details of SAXS results

To interpret the shoulder observed at q = 0.07–0.1 Å^{-1}, we fitted the scattering function of a model particle (discs of diameter D and thickness T) to the relevant part of the experimental SAXS curve (Figure S9). The resulting parameters are ascribed to the building blocks of the large particles. The radius of gyration, mass, volume, and specific surface were determined using previously published formulae.[1]

To provide detailed insight into the size of the particles, the results are presented as weighted diameters of the spherical particles. Due to the different moments in the size distribution, the following inequalities should be fulfilled:[2]

$$D_R \geq D_V \geq D_M \geq D_S$$

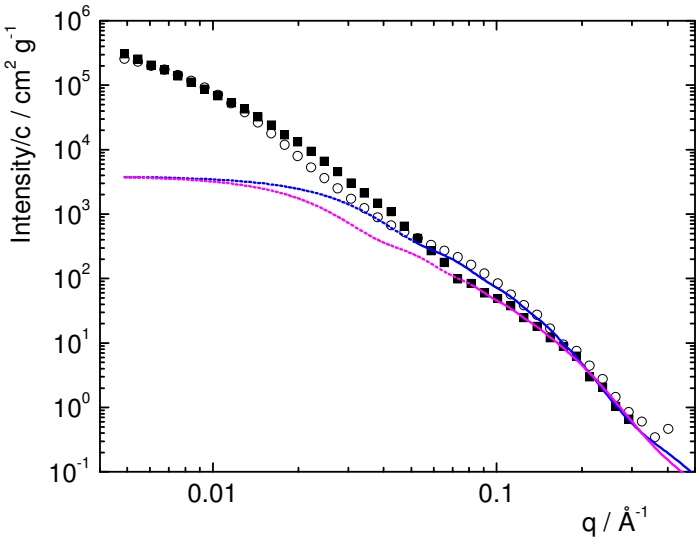

Figure S9. Experimental SAXS curves of the ZnO dispersions in *n*BuOH prepared at 60 °C (full squares) and 100 °C (open circles) (6 - 9 g L^{-1}). The observed shoulder is ascribed to the scattering contribution of sub-particles and fitted to the scattering function of disc-model particle (solid line) and extrapolated to the q-range where the dominant scattering contribution originates from large spherical particles (dotted line).

The determined parameters for the ZnO dispersion are summarized in Table S1. The values of D_R, D_V, and D_M range between 29 and 67 nm and are representative of the large particles, while D_S (6–9 nm) reflects the presence of small heterogeneities (sub-particles or the internal structure of the large particles). The clear inequalities between the mean diameters reveal

rather strong polydispersity. The diameters D_V and D_M depend on the same moments, but D_V is larger if the particles are swollen. Therefore, the sizable difference between D_V and D_M can be explained by the swelling of the large particles. The degree of swelling, given in Table S1, was calculated as follows:

$$DoS = (D_V / D_M)^3$$

Table S1. Structure parameters of ZnO dispersions in *n*BuOH: Mean diameters determined from the radius of gyration (D_R), volume (D_V), mass (D_M), and specific surface (D_S), respectively; degree of swelling of the large particles (DoS); thickness (T) and diameter (D) of the sub-particles.

Temperature / °C	D_R /nm	D_V /nm	D_M /nm	D_S /nm	DoS	T /nm	D /nm
60 [a]	65	42	36	7	1.5	2.3	17
80 [a]	52	35	29	9	1.6	2.5	23
100 [a]	67	38	32	8	1.7	1.5	18
60 [b]	65	38	32	6	1.6	2.2	16

[a] Stirring at given temperature for 24 h. [b] Shaking at 60°C for 24 h.

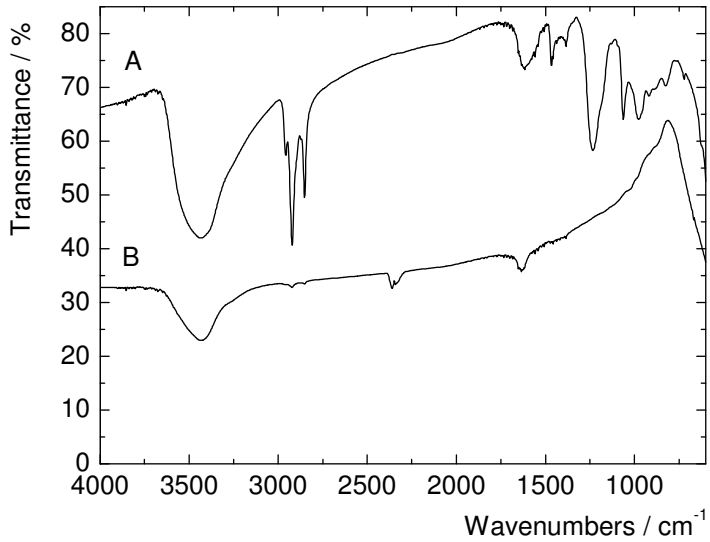

Figure S10. FTIR spectra of ZnO prepared at 60 °C in *n*BuOH (A) and the same sample after calcination at 1300 °C (after the TGA/DTA analysis) (B). The spectrum B is vertically shifted for better clarity.

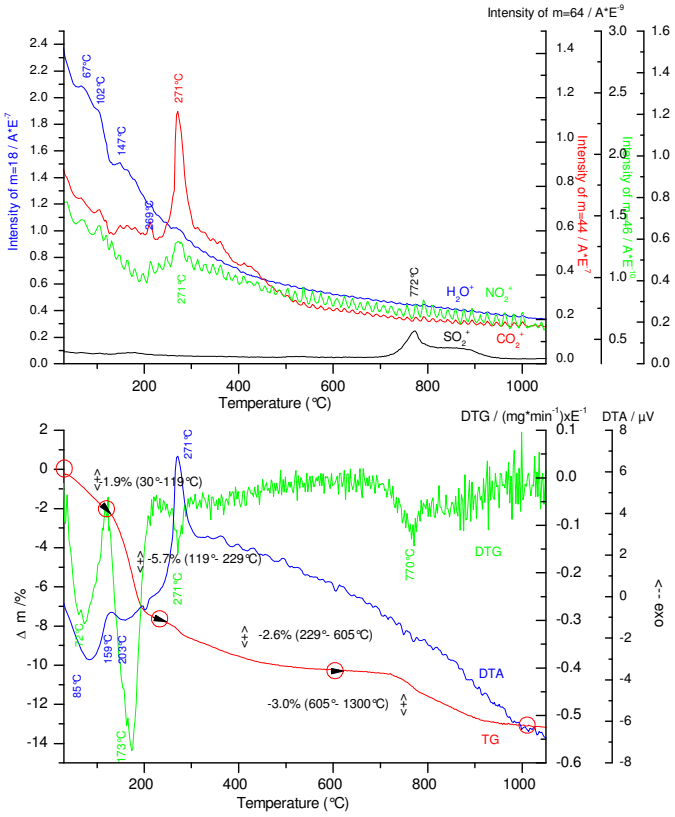

Figure S11. TGA/DTA curves and the evolution of gases for ZnO prepared at 60°C in *n*BuOH and dried at room temperature.

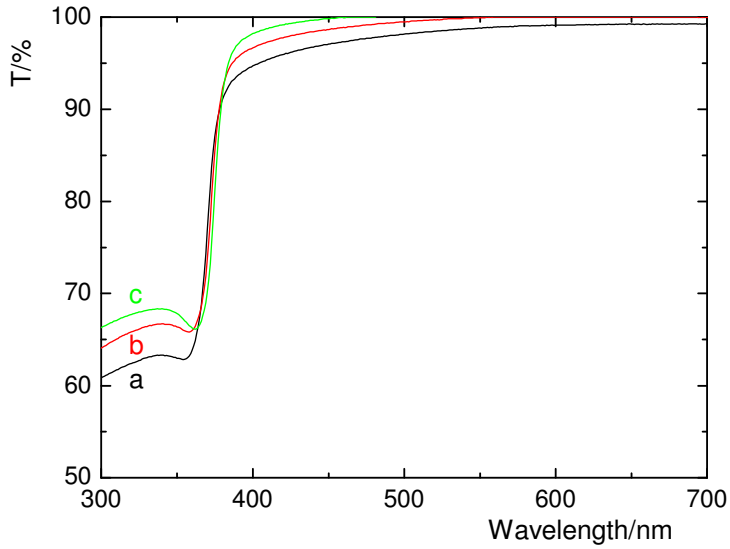

Figure S12. UV-visible absorption spectra of the films on quartz plates: (a) As-prepared film, two layers; (b) After treatment at 300 ^{o}C for 2 hours; (c) After treatment at 700 ^{o}C for 2 hours The films were deposited by dip-coating of chloroform ZnO dispersions.

XRD patterns of ZnO

The diffraction patterns of the ZnO powders were collected using a PANalytical X´Pert PRO diffractometer equipped with a conventional X-ray tube (CuKα 40 kV, 30 mA, line focus) in transmission mode. An elliptic focusing mirror, 0.5° divergence slit, 0.5° anti-scatter slit, 0.02 rad Soller slit, and 20 mm mask were used in the primary beam. A fast linear position sensitive detector PIXcel with an anti-scatter shield and 0.02 rad Soller slit was used in the diffracted beam. All patterns were collected in the range between 1 and 88° (2 Θ) with a step of 0.0065° (510 sec/step).

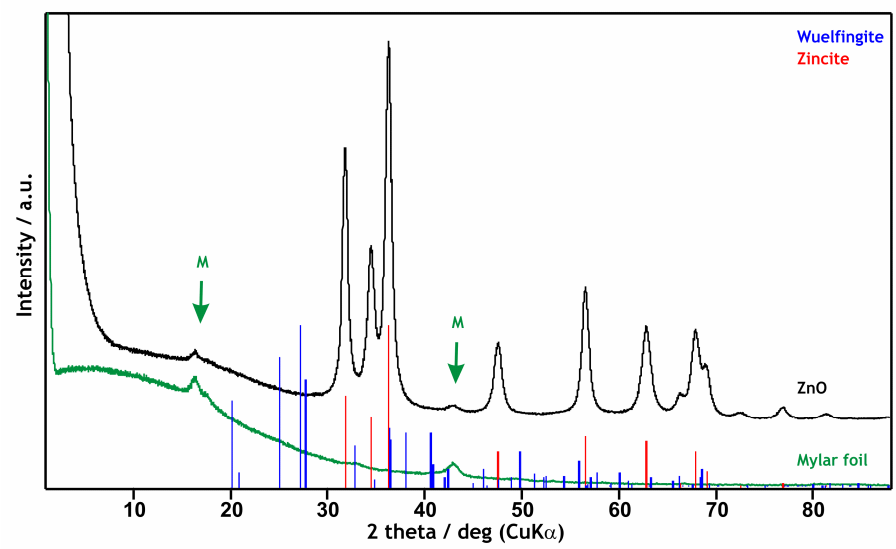

Figure S13. Powder XRD patterns of the ZnO powder (black line) are compared with the diffractions of zincite (red) (ZnO, JCPDS 01-089-0510) and wuelfingite (blue) ($Zn(OH)_2$, JCPDS 00-038-385). The patterns confirm that the starting LZH-DS is completely transformed into ZnO. There are no signs of wuelfingite as suggested by the referee. The diffractions labeled as M (green line) are caused by a Mylar foil used as a sample support.

References

(1) *Small-Angle X-Ray Scattering* (eds.: Glatter, O.; Kratky, O.), Academic Press Inc., London, **1982**.

(2) Pleštil, J.; Baldrián, J. *Czech. J. Phys.* **1976**, *B26*, 514-527.